LETTERS

Non-equilibration of hydrostatic pressure in blebbing cells

Guillaume T. Charras[1], Justin C. Yarrow[1], Mike A. Horton[2], L. Mahadevan[1,3,4] & T. J. Mitchison[1]

Current models for protrusive motility in animal cells focus on cytoskeleton-based mechanisms, where localized protrusion is driven by local regulation of actin biochemistry[1–3]. In plants and fungi, protrusion is driven primarily by hydrostatic pressure[4–6]. For hydrostatic pressure to drive localized protrusion in animal cells[7,8], it would have to be locally regulated, but current models treating cytoplasm as an incompressible viscoelastic continuum[9] or viscous liquid[10] require that hydrostatic pressure equilibrates essentially instantaneously over the whole cell. Here, we use cell blebs as reporters of local pressure in the cytoplasm. When we locally perfuse blebbing cells with cortex-relaxing drugs to dissipate pressure on one side, blebbing continues on the untreated side, implying non-equilibration of pressure on scales of approximately 10 μm and 10 s. We can account for localization of pressure by considering the cytoplasm as a contractile, elastic network infiltrated by cytosol. Motion of the fluid relative to the network generates spatially heterogeneous transients in the pressure field, and can be described in the framework of poroelasticity[11,12].

Blebs are large, approximately spherical deformations of the cell surface that form and disappear on a timescale of tens of seconds. Although less studied than lamellipodial or filopodial protrusion, blebbing is a common phenomenon during apoptosis[13], cytokinesis[14,15] and cell movement[16,17]. Blebs are thought to be initiated by rupture of the plasma membrane from the underlying cytoskeleton (Supplementary Fig. 3), followed by inflation of the detached membrane by intracellular fluid flow[18,19]. Subsequent bleb retraction is driven by assembly and contraction of a cortex within the newly formed bleb. Blebbing requires non-uniform behaviour of the membrane and cortex that must reflect either a globally uniform hydrostatic pressure combined with local nucleation of membrane detachment from the cytoskeleton, or non-uniform pressure leading to local rupture of membrane–cytoskeleton attachments in regions of high pressure. To distinguish these possibilities, we studied the effect of local disruption of cortical contraction or integrity induced by drug perfusion over part of a cell, in a filamin-depleted melanoma cell line (M2) that blebs extensively and continuously[20].

We first confirmed that the cell volume stays approximately constant during blebbing (Supplementary Data, Supplementary Video 12 and Supplementary Fig. 4)[18], implying that blebbing is driven primarily by flow of fluid within the cell rather than water crossing the plasma membrane. We then confirmed that bleb inflation represents ballooning out of the plasma membrane when it detaches from the actin cortex by simultaneously imaging the cortex and the cell membrane (Supplementary Fig. 3). During bleb inflation, green fluorescent protein (GFP)-tagged actin was not enriched at the bleb surface compared to its interior, implying lack of a cytoskeleton in the bleb (Fig. 1a, $t = 0$ and 22 s). As inflation slowed, a cortical cytoskeleton assembled underneath the bleb membrane, evidenced by a rim of actin fluorescence (Fig. 1a, $t = 62$ s); simultaneously, the cortex at the base of the bleb disassembled (Supplementary Fig. 3). As the bleb retracted, its actin rim became more pronounced, and often wavy or buckled, suggesting that the cortex contracts as the bleb shrinks (Fig. 1a, $t = 72$ s)[19]. GFP–myosin II regulatory light chain (MRLC) was recruited to the newly forming cortex of the bleb simultaneous with actin (Fig. 1b; see also Supplementary Video 10)[13,21], consistent with myosin II driving contraction. Increasing extracellular osmolarity made blebs smaller, whereas decreasing it made them larger[22] (Fig. 1; see also Supplementary Video 1). Increasing membrane rigidity by crosslinking the glycocalix polysaccharides with wheat germ agglutinin (WGA)[23] inhibits blebbing (Supplementary Video 2). These observations, together with drug studies discussed below, support the following qualitative model for bleb dynamics[19]. Cortical acto-myosin contracts (Supplementary Videos 10 and 11), generating hydrostatic pressure that causes a patch of plasma membrane to tear free from its attachment to the cortical cytoskeleton. This patch of cytoskeleton-free membrane rapidly inflates as cytosol flows in, with its base enlarging by further tearing (Supplementary Fig. 3). Later, inflation slows and a mesh of actin and myosin II assembles in the bleb to form a contractile cortex attached to the plasma membrane (Fig. 1b). Finally, contraction of this cortical mesh causes the bleb to shrink, driving the extruded cytosol back into the cell body.

To find inhibitory small molecules, we screened a library of known biologically active compounds for rapid inhibition of blebbing. After characterizing their effects in bath treatment, selected drugs and osmolytes were applied locally to cells by injecting medium containing inhibitor via a micropipette into a laminar fluid flow[24,25]. The treated region was visualized by adding a fluorescent tracer to the pipette medium, whereas blebbing was observed using differential interference contrast (DIC) microscopy. During local perfusion, we typically bathed 20–33% of the cell area. We confirmed local application by visualizing local deposition of a fluorescent lectin (WGA–Alexa 488; Fig. 2a, $t = 430$ s). For each drug, local perfusion experiments were repeated until one of the following behaviours was observed reproducibly ($N \geq 5$): (1) local perfusion of drug inhibited blebbing locally; (2) local perfusion had both a local and global effect on blebbing; (3) local perfusion did not inhibit blebbing but whole-cell treatment did.

The effect of local perfusion could be classified into three categories. The first is treatments that locally inhibited blebbing but allowed the untreated part of the cell to bleb normally (Fig. 2; see also Supplementary Table 1 and Supplementary Videos 3–6). As expected, agents that increased membrane rigidity (WGA) or osmotic pressure (sucrose) had this effect (Fig. 2a, b). These agents locally increase the physical forces that oppose blebbing. Notably, drugs that block generation of contractile force also had local inhibitory effects, including inhibitors of myosin II (blebbistatin[21]) and ROCK1 (Y-27632 and 3-(4-pyridyl)indole[26]), a kinase that activates

[1]Department of Systems Biology, Harvard Medical School, Boston, Massachusetts 02115, USA. [2]London Centre for Nanotechnology, University College London, London WC1E 6JF, UK. [3]Division of Engineering and Applied Sciences, and [4]Department of Organismic and Evolutionary Biology, Harvard University, Cambridge, Massachusetts 02138, USA.

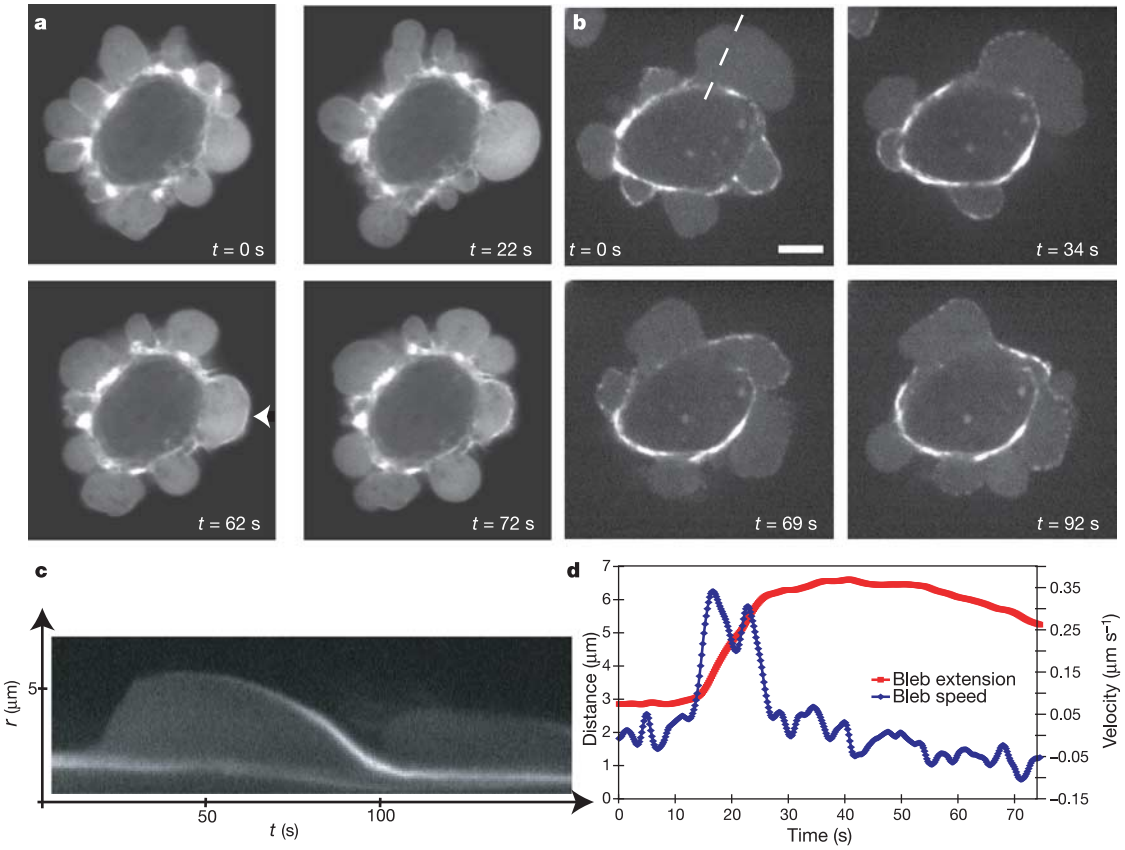

Figure 1 | Localization of GFP–actin and GFP–MRLC in blebs shows that expansion is a passive process and retraction an active process necessitating actin and MRLC. All images were acquired by confocal microscopy. Scale bar, 5 μm. **a**, GFP–actin-transfected cell. During bleb expansion, the bleb rim does not appear to be enriched in GFP–actin compared to the bleb interior ($t = 0$ s and $t = 22$ s). Once expansion has halted, an actin-rich rim forms at the bleb surface ($t = 62$ s, arrowhead) and retraction begins. As retraction proceeds, the actin rim becomes wavy, suggesting that the cortex contracts as the bleb shrinks ($t = 72$ s). **b**, GFP–MRLC-transfected cell. Just after expansion has stopped, the bleb surface does not appear to be enriched in GFP–MRLC ($t = 0$ s). MRLC then accumulates in discrete foci ($t = 34$ s) and retraction starts ($t = 69$ s). As retraction ends, MRLC forms a continuum along the bleb rim ($t = 92$ s). **c**, Kymograph of the expansion and retraction of the bleb in **b** (dashed line). As the bleb expands, there is no accumulation of MRLC at the bleb apex. As retraction proceeds, MRLC accumulates at the bleb. Bleb extension (r) is on the y axis. **d**, Graph of the bleb extension and bleb velocity as a function of time for the bleb shown in **c**. The maximal bleb extension is approximately 3.5 μm (maximal speed of expansion about 0.35 μm s^{-1}, speed of retraction about 0.1 μm s^{-1}).

myosin II (Fig. 2c, d). The second category is treatments that caused a combination of local and global effects, as seen with the F-actin-disrupting agents cytochalasin D and latrunculin B (Fig. 3a; see also Supplementary Video 7). Within seconds of local drug application, there was a global increase in bleb size (Fig. 3a, $t = 75$ s). Then, blebbing ceased in the treated area and existing blebs were not retracted, whereas blebbing continued in the untreated area at a slower rate than before drug application (Fig. 3a, $t = 315$ s). The third category is treatments that only had an effect when the whole cell was treated. Inhibitors of several other protein kinases had this effect (Fig. 3b, c; see also Supplementary Videos 8 and 9). For local perfusion to perturb the cytoplasm locally, membrane crossing must be fast compared with intracellular diffusion of the drug or drug–target complex[27]. Thus, failure to see a local effect of a drug cannot be interpreted in terms of local versus global action of its target.

The local effects of myosin-II-inhibiting drugs (Fig. 2c, d) show that the acto-myosin cortex acts locally to promote blebbing. This could be because contraction locally nucleates blebs, while hydrostatic pressure is uniform, or because pressure generated by contraction only acts locally to extrude blebs, implying that it does not globally equilibrate. Local inhibition of blebbing by actin-depolymerizing drugs (Fig. 3a) favours the latter hypothesis. If pressure equilibrated across the cell, the drug-treated side, where the cortex is softer, should swell preferentially, inhibiting blebbing on the untreated side. Because this does not happen, we conclude that hydrostatic pressure does not equilibrate across single M2 cells on time- and length-scales relevant to motility.

Current models of the cytoplasm[9,10] cannot account for spatio-temporally localized variations in hydrostatic pressure. We therefore propose a new description of the cytoplasm based on poro-elasticity[11,12]. We consider the cytoplasm to be composed of a porous, actively contractile, elastic network (cytoskeletal filaments, organelles and ribosomes), infiltrated with an interstitial fluid (that is, the cytosol, comprising water, ions and soluble proteins), similar to a fluid-filled sponge. Contraction of the acto-myosin cortex creates a compressive stress on the cytoskeletal network, leading to a spatially localized increase in hydrostatic pressure (Fig. 4a). In response, the cytosol flows out of the network, and if it finds a region where the membrane is weakly attached to the cortex; the resulting pressure can lead to membrane detachment and bleb inflation (Fig. 4b; see also Supplementary Fig. 3). With a poroelastic description of the cytoplasm, hydrostatic pressure does not instantaneously propagate through the network. Instead, it diffuses over a length $x \approx \sqrt{Dt}$ during a time t, with the diffusion constant $D = \frac{kK}{\phi}$ determined by an appropriately defined elastic bulk modulus K, the hydraulic permeability of the network k, and the local volume fraction of fluid ϕ (see Supplementary Information). The diffusion constant D dictates the time needed for the effect of a local contractile force to be felt in

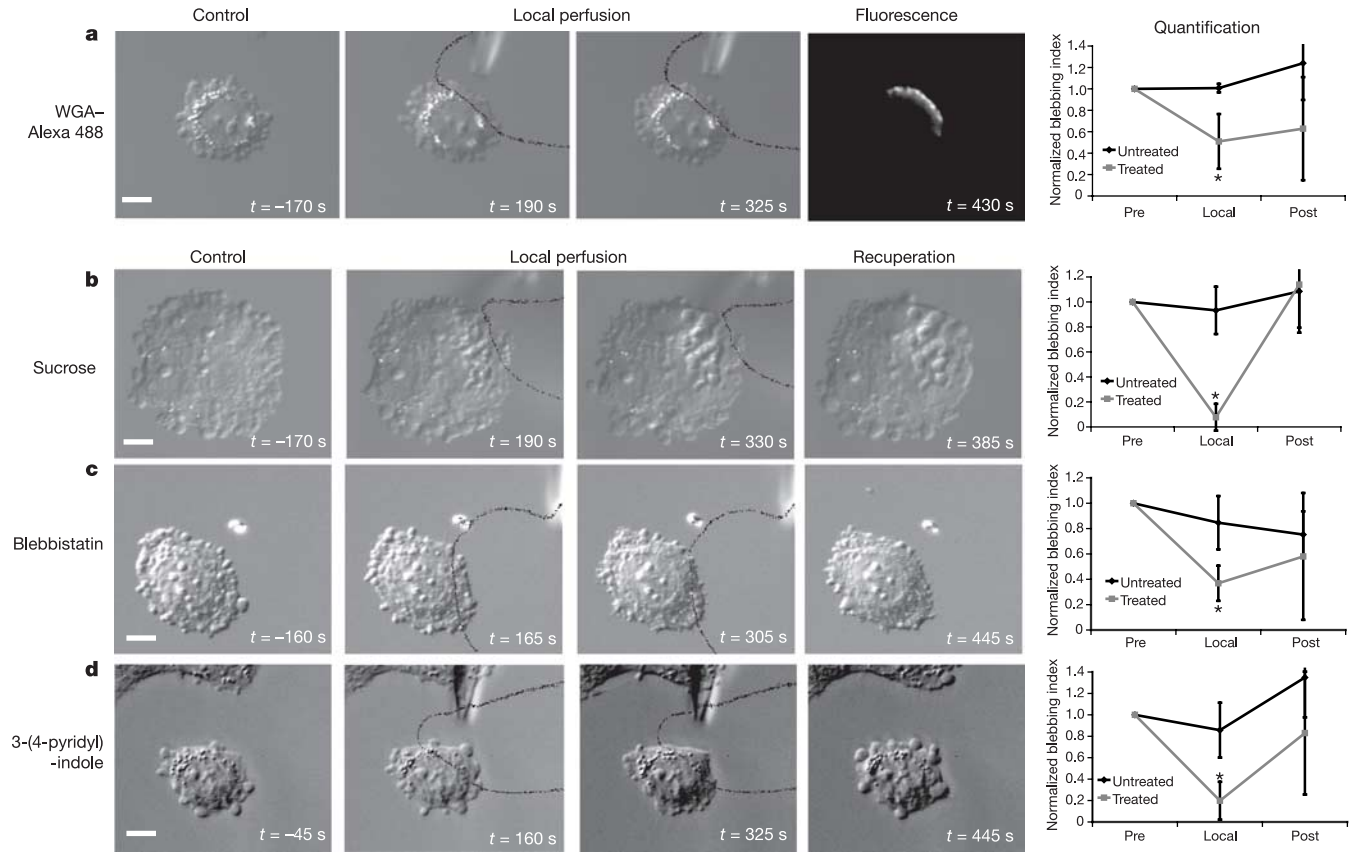

Figure 2 | Local perfusion can locally inhibit blebbing. In all cases, before application of treatment the cells blebbed profusely around their periphery.Within 2–3 min of application, blebbing ceases in the area of application but continues undisturbed in the rest of the cell. In some cases, when the local perfusion was halted ($t_{off} = 350$ s in all cases), cells recovered and blebbed normally. **a**, Local perfusion of WGA–Alexa 488. WGA–Alexa 488 was only incorporated in the region of the cell that was exposed to flow from the micropipette. **b**, Local perfusion of 300 mM sucrose solution. Vacuoles form in the vicinity of the perfused region. **c**, Local inhibition of myosin II ATPase by local perfusion of blebbistatin. **d**, Local inhibition of ROCKI by 3-(4-pyridyl)indole. Black lines delineate the flow out of the micropipette. On each image, timing relative to local application of treatment is given. The normalized blebbing indices (right) show the evolution over time of blebbing in the region exposed to inhibitor and in the free region. Error bars show the standard deviation. Asterisks denote significant changes in the blebbing index when compared with the initial blebbing index. Scale bars, 10 μm.

other parts of the cell. Using a typical timescale for bleb inflation of $t \approx 10$ s and realistic values for the various parameters (Supplementary Information), we find $x \approx 15$–30 μm. Hence, hydrostatic pressure can be strongly non-equilibrated in cells on a timescale of approximately 10 s and a length scale of about 10 μm—scales that are relevant to a variety of motile behaviours. Bleb formation reduces this length scale by allowing the fluid to flow, with less resistance, into the blebs instead of through the network. Local inhibition of blebbing is possible because opposite sides of the cells are effectively isolated from each other with respect to equilibration of pressure on a timescale of seconds.

Our poroelastic model could have important implications for other types of cell motility, because it implies that hydrostatic pressure can be generated and used locally to power shape change in animal cells. Leading-edge protrusion is typically coupled to actin polymerization[1–3], but hydrodynamic force could work together with polymerization force to power protrusion[7,8], and fluid flow could drive actin subunits forwards at a faster rate than that predicted by pure diffusion[28]. Localized hydrostatic pressure transients could be generated locally near the front of polarized cells by local recruitment and activation of myosin II as in blebbing, or of plasma membrane ion transporters (such as NHE1 (ref. 29)) that can trigger swelling through influx of an osmolyte (such as Na^+). Overall, our work shows that cytosolic fluid dynamics must be integrated with protein dynamics if we are to really understand cell motility.

METHODS

Local perfusion. Local perfusion was performed by injecting medium with the desired concentration of drug into a laminar fluid flow via a glass micropipette with a 1–2-μm diameter. Thin-walled borosilicate micropipettes (0.9-mm inner diameter) were pulled on a Sutter P87 pipette puller (Sutter instrument company). Coverslips on which cells had been cultured were affixed onto the bottom of the laminar fluid flow chamber (blueprint available upon request) with a 1:1:1 mix of vaseline, lanolin and paraffin. Laminar flow was created by feeding medium into the flow chamber at a constant rate of 30 ml h^{-1} with a syringe pump. A constant fluid level was maintained by aspirating the supernatant via a vacuum pump. The flow chamber consisted of a reservoir with a small opening (0.7 mm) that enables medium to enter the open part of the chamber and delivers a flow of approximately 30 μm s^{-1} in the vicinity of this entrance. For the flow to be sufficiently rapid to carry drug away, the target cells needed to be chosen within 200 μm of the reservoir opening. All experiments were performed at room temperature in Leibovitz-L15 medium with 10% 80:20 mix of donor calf serum:fetal calf serum. The microinjected solution was made up of medium with the desired concentration of drug and 0.1 μM of tetramethylrhodamine-isothiocyanate (TRITC, used as a fluorescent tracer) and filtered using a centrivac tube (Millipore). The micropipettes were backfilled with the solution and mounted onto a pipette holder attached to a three-axis oil hydraulic micromanipulator (Narishige). A pressure regulator (Eppendorf 5242, Eppendorf AG) set between 40 and 80 hPa was used to control flow from the micropipette.

Time-lapse video microscopy of the local perfusion experiments was performed as described in Supplementary Methods, except that in addition to DIC images, fluorescence images were also acquired (TRITC filters to visualize flow lines and fluorescein-isothiocyanate (FITC) filters to visualize WGA–Alexa

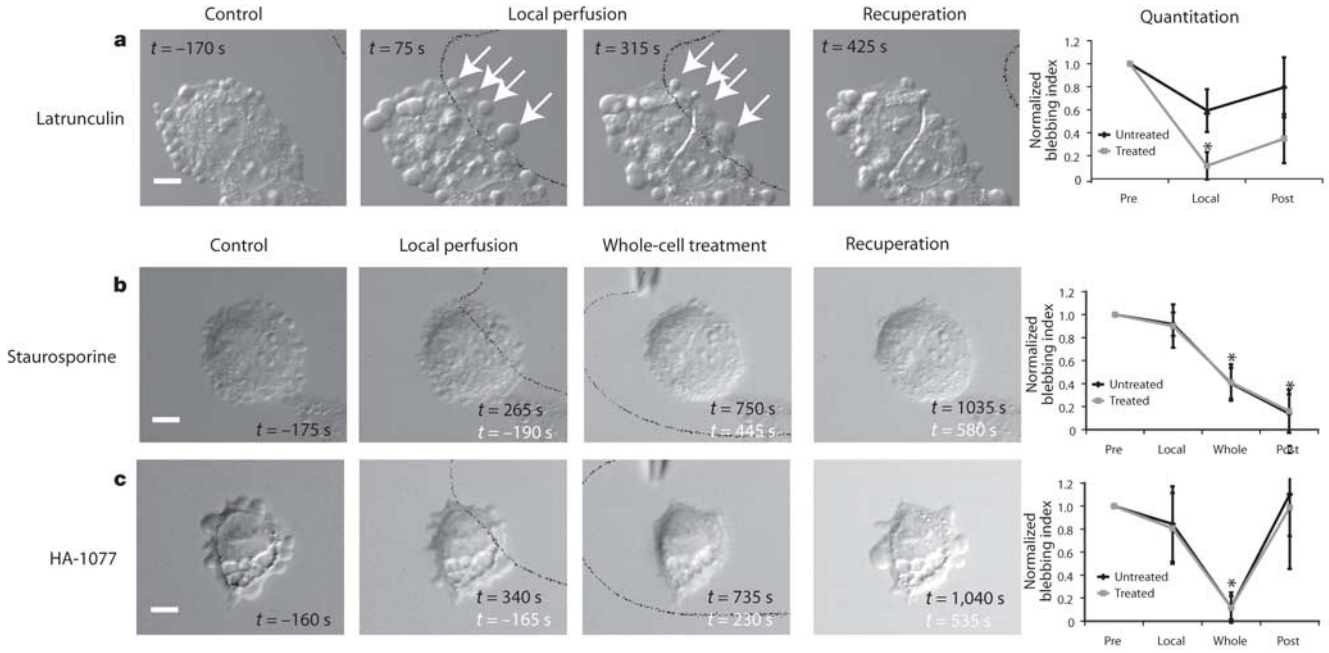

Figure 3 | **Compounds with dual or global effects on blebbing.** **a**, Local perfusion with latrunculin B has a dual effect. When latrunculin B is applied locally, bleb size increases globally ($t = 75$ s), and bleb dynamics cease in the treated area ($t = 75$ s and $t = 315$ s). Elsewhere, expansion and retraction continue. **b**, Global perfusion of staurosporine is necessary to inhibit blebbing. Before perfusion ($t = -175$ s) and after 395 s of local perfusion with staurosporine, blebbing is unperturbed throughout the cell. When staurosporine is applied to the whole cell (white text, $t = 445$ s), blebbing ceases. **c**, Global perfusion of HA-1077 is necessary to inhibit blebbing. After 340 s of local HA-1077 application, blebbing is unperturbed. When the whole cell is exposed to inhibitor ($t = 230$ s, white text), blebbing ceases. When perfusion is halted, blebbing is restored ($t = 535$ s, white text). Black lines delineate the flow coming out of the micropipette. Black text gives time relative to local application; white text gives time relative to global application. The normalized blebbing indices show the evolution over time of blebbing in the region exposed to inhibitor and in the free region. Error bars show the standard deviation. Asterisks denote significant changes in the blebbing index when compared with the initial blebbing index. Scale bars, 10 μm.

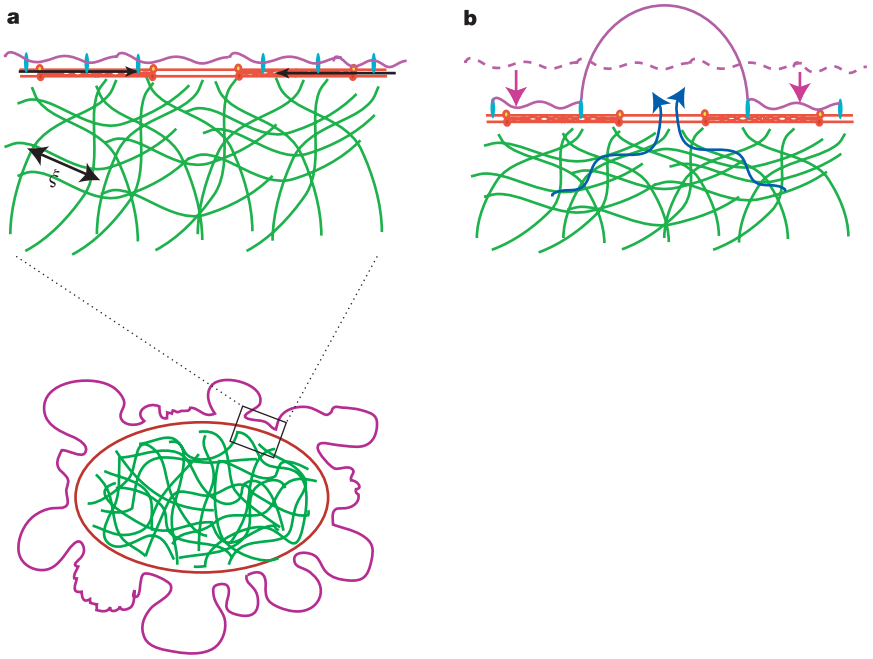

Figure 4 | **Poroelastic description of blebbing.** In all drawings, the actin cortex is drawn in red, the membrane is mauve and the cytoskeletal meshwork is green. **a**, In blebbing cells, a local contraction of myosin II (black arrows) associated with the actin cortex leads to a shortening of the cortical periphery and therefore to a compression of the cytoskeletal network that fills the cell. The cytoskeletal network is porous and has an average pore size ξ. The compression of the cytoskeletal meshwork creates a hydrostatic pressure in the vicinity of the region of contraction and can lead to bleb nucleation and expansion. **b**, Contraction of the actin cortex leads to a compression of the cytoskeletal network (the dashed mauve line indicates the original position of the cell surface) and drives flow of cytosol in the opposite direction (blue arrows). If there is a local defect in membrane–cytoskeleton attachment, a bleb is extruded. Bleb expansion is opposed by two forces: extracellular osmotic pressure and membrane tension.

488). Exposure times were approximately 200 ms for DIC images, 600 ms for TRITC images and about 250 ms for FITC images. Images were acquired every 5 s with a × 20 objective using Metamorph (Universal Imaging Corp.). During a typical local perfusion experiment, about 30 images (approximately 150 s) were acquired before drug exposure. Then, the cell was exposed to drug for about 70 images (approximately 350 s), finally the cell was allowed to recover for 20 frames (about 100 s). When no local inhibition was observed, a whole-cell treatment was performed. This time, the cell was observed for 30 frames to ensure that it still blebbed, the whole cell was exposed to drug for 70 frames, and recovered for 20 frames. Initial concentrations of drug in the microinjected fluid were chosen to be two to three times those needed in bulk solution[25]. When no inhibition was observed when the whole cell was exposed to drug, the drug concentration in the micropipette was increased. When whole-cell inhibition was observed with only local perfusion, the drug concentration was decreased.

Post-hoc flow lines were superimposed onto the DIC images using Metamorph. The fluorescence images were assigned a threshold and intensities of 25% of the maximum intensity were converted to a binary image that was inverted and superimposed onto the DIC image using an AND operator.

Analysis and quantification of local perfusion assays. Each cell was divided into two regions: the treated region where local perfusion was applied, and the control untreated region. Each experiment was divided into different periods: (1) before the application of drug; (2) during local application of drug; (3) after application of drug; and, if need be, (4) during whole-cell treatment. The number of blebs occurring in each region for each period was counted manually. A blebbing index was computed for each region as follows: $B = \frac{N_{\text{blebs}}}{Lt}$, where N_{blebs} is the number of blebs observed during a given period t over a given perimeter L. These blebbing indices were used to compare the treated region to the untreated region before application of inhibitor, and the blebbing in either region during and after application of inhibitor to the blebbing in that region before application. Populations were compared with a Student's t-test and the level of significance was taken to be $P < 0.01$. For graphic output (Figs 2 and 3), the evolution of the blebbing indices was normalized to their values before application of local perfusion. In all cases, the blebbing index in the treated and untreated region was not significantly different before application of inhibitor ($P > 0.3$).

Received 19 January; accepted 15 March 2005.

1. Mahadevan, L. & Matsudaira, P. Motility powered by supramolecular springs and ratchets. *Science* **288,** 95–100 (2000).
2. Rafelski, S. M. & Theriot, J. A. Crawling toward a unified model of cell mobility: spatial and temporal regulation of actin dynamics. *Annu. Rev. Biochem.* **73,** 209–239 (2004).
3. Mogilner, A. & Oster, G. Polymer motors: pushing out the front and pulling up the back. *Curr. Biol.* **13,** R721–R733 (2003).
4. Messerli, M. A. & Robinson, K. R. Ionic and osmotic disruptions of the lily pollen tube oscillator: testing proposed models. *Planta* **217,** 147–157 (2003).
5. Money, N. P. & Harold, F. M. Extension growth of the water mold Achlya: interplay of turgor and wall strength. *Proc. Natl Acad. Sci. USA* **89,** 4245–4249 (1992).
6. Harold, F. M. Force and compliance: rethinking morphogenesis in walled cells. *Fungal Genet. Biol.* **37,** 271–282 (2002).
7. Tilney, L. G. & Inoue, S. Acrosomal reaction of the Thyone sperm. III. The relationship between actin assembly and water influx during the extension of the acrosomal process. *J. Cell Biol.* **100,** 1273–1283 (1985).
8. Condeelis, J. Life at the leading edge: the formation of cell protrusions. *Annu. Rev. Cell Biol.* **9,** 411–444 (1993).
9. Boal, D. H. *Mechanics of the Cell* (Cambridge Univ. Press, Cambridge, UK, 2002).
10. Drury, J. L. & Dembo, M. Hydrodynamics of micropipette aspiration. *Biophys. J.* **76,** 110–128 (1999).
11. Biot, M. General theory of three-dimensional consolidation. *J. Appl. Phys.* **12,** 155–164 (1941).
12. Wang, H. *Theory of Linear Poroelasticity with Applications to Geomechanics and Hydrogeology* (Princeton Univ. Press, Princeton, New Jersey, 2000).
13. Mills, J. C., Stone, N. L., Erhardt, J. & Pittman, R. N. Apoptotic membrane blebbing is regulated by myosin light chain phosphorylation. *J. Cell Biol.* **140,** 627–636 (1998).
14. Fishkind, D. J., Cao, L. G. & Wang, Y. L. Microinjection of the catalytic fragment of myosin light chain kinase into dividing cells: effects on mitosis and cytokinesis. *J. Cell Biol.* **114,** 967–975 (1991).
15. Burton, K. & Taylor, D. L. Traction forces of cytokinesis measured with optically modified elastic substrata. *Nature* **385,** 450–454 (1997).
16. Trinkaus, J. P. Surface activity and locomotion of Fundulus deep cells during blastula and gastrula stages. *Dev. Biol.* **30,** 69–103 (1973).
17. Friedl, P. & Wolf, K. Tumour-cell invasion and migration: diversity and escape mechanisms. *Nature Rev. Cancer* **3,** 362–374 (2003).
18. Albrecht-Buehler, G. Does blebbing reveal the convulsive flow of liquid and solutes through the cytoplasmic meshwork? *Cold Spring Harb. Symp. Quant. Biol.* **46,** 45–49 (1982).
19. Cunningham, C. C. Actin polymerization and intracellular solvent flow in cell surface blebbing. *J. Cell Biol.* **129,** 1589–1599 (1995).
20. Cunningham, C. C. *et al.* Actin-binding protein requirement for cortical stability and efficient locomotion. *Science* **255,** 325–327 (1992).
21. Cheung, A. *et al.* A small-molecule inhibitor of skeletal muscle myosin II. *Nature Cell Biol.* **4,** 83–88 (2002).
22. Dai, J. & Sheetz, M. P. Membrane tether formation from blebbing cells. *Biophys. J.* **77,** 3363–3370 (1999).
23. Evans, E. & Leung, A. Adhesivity and rigidity of erythrocyte membrane in relation to wheat germ agglutinin binding. *J. Cell Biol.* **98,** 1201–1208 (1984).
24. Popov, S., Brown, A. & Poo, M. M. Forward plasma membrane flow in growing nerve processes. *Science* **259,** 244–246 (1993).
25. O'Connell, C. B., Warner, A. K. & Wang, Y. Distinct roles of the equatorial and polar cortices in the cleavage of adherent cells. *Curr. Biol.* **11,** 702–707 (2001).
26. Yarrow, J. C., Totsukawa, G., Charras, G. T. & Mitchison, T. J. Screening for cell migration inhibitors via automated microscopy reveals a rho-kinase inhibitor. *Chem. Biol.* **12,** 385–395 (2005).
27. Takayama, S. *et al.* Selective chemical treatment of cellular microdomains using multiple laminar streams. *Chem. Biol.* **10,** 123–130 (2003).
28. Zicha, D. *et al.* Rapid actin transport during cell protrusion. *Science* **300,** 142–145 (2003).
29. Baumgartner, M., Patel, H. & Barber, D. L. Na(+)/H(+) exchanger NHE1 as plasma membrane scaffold in the assembly of signaling complexes. *Am. J. Physiol. Cell Physiol.* **287,** C844–C850 (2004).

Supplementary Information is linked to the online version of the paper at www.nature.com/nature.

Acknowledgements The authors would like to acknowledge the Nikon Imaging Centre at Harvard Medical School and, in particular, J. Waters. The authors would also like to acknowledge J. Horn at the HMS machine shop for manufacturing the perfusion chamber. G.T.C. was in receipt of a Wellcome Trust Overseas Fellowship. M.A.H. is supported by a Programme Grant from the Wellcome Trust. L.M. was supported by NSF-MRSEC at Harvard University. This work was supported by a grant from the NIH to T.J.M.

Author Information Reprints and permissions information is available at npg.nature.com/reprintsandpermissions. The authors declare no competing financial interests. Correspondence and requests for materials should be addressed to G.T.C. (gcharras@hms.harvard.edu).

Material and Methods

Supplementary Theory

Here, we give a simple theoretical interpretation of the experimental observations. On length-scales large compared to the pore size (Figure 4A), we can treat the cytoplasm as a fluid-solid composite medium with an important difference from traditional continuum models: there can be relative motion between the network and the fluid. However, since the Reynolds number of the flow is negligible and the deformations of the network are very slow, we ignore inertial effects. Here we treat this limit at the level of scaling laws in a one-dimensional geometry for conceptual simplicity, leaving a more complete description to the future (for a brief description of the derivation of the theory and some implications in confined geometries, see Skotheim and Mahadevan[1]). Stress balance in a one-dimensional slice of the network yields $\partial_x \sigma + f = 0$ where $\sigma = K\partial_x u - \phi p$ is the one-dimensional stress in a composite linear elastic network bathed in a viscous fluid with K the drained bulk modulus of the network, p the fluid pressure, and f the body force due to the contractile motors in the gel. Here, the pressure is the dominant contribution from the fluid stress due to the large disparity between pore size and system size (the cell). Assuming incompressibility of the constituent fluid and the material of the network, continuity demands that the average velocity of the fluid relative to the solid network $\varphi v = -(1-\varphi)\partial_t u$, where u is the displacement of the network, and φ is the local fluid volume fraction. Darcy's law applied to a poroelastic continuum yields a relation between the macroscopic pressure gradient $\partial_x p$ and the relative fluid velocity $\varphi(v - \partial_t u) = -k\partial_x p$, with k the hydraulic permeability of the cytoskeleton. Using the equation of continuity in Darcy's law and substituting the result into the stress balance yields a diffusion equation for the displacement (and hence the stress) in the network: $D\partial_{xx} u + kf = \partial_t u$, with the diffusion constant $D = \frac{kK}{\phi}$ determined by the elastic and hydraulic properties of the network. Ignoring the detailed solution of the resulting initial boundary value problem for now, here we focus on the scaling aspects of the solution. We see that following an impulsive contractile stress due to the motors, say, the stress does not instantaneously propagate through the cytoskeleton, but instead diffuses through it over a length $x \approx \sqrt{Dt}$ during a time t. For a fluid-saturated porous medium with a small fluid volume fraction, the hydraulic permeability is $k \approx \frac{\xi^2}{\mu\phi^{1/3}}$ where ξ is the pore size, and μ the viscosity of the cytosol. Using an experimentally measured elastic modulus K~ 2 kPa (Supplemental data), a cytosolic viscosity μ~5.10^{-2} Pa.s based on the diffusion of molecules up to 100Å (in particular G-actin, which diffuses into blebs to recreate the actin cortex) [1-3], a pore size ξ~10-20 nm derived from examination of electron micrographs of the cell line and size-exclusion experiments [4-6], a fluid fraction ϕ~0.2 [7], and a typical time-scale for bleb extrusion of t~10s, we find x~15-30μm. Hence, hydrostatic pressure can be strongly non-equilibrated in cells on a time-scale of ~10s and a length-scale of ~10μm: scales that are relevant to a variety of motile behaviors. Experimental determination of the pore size ξ will be essential as it is a key parameter in setting the diffusion length, since it is a crucial determinant of both the hydraulic permeability and the elasticity of the network. Bleb formation reduces this length-scale by allowing the fluid to flow,

with less resistance, into the blebs instead of through the network. Local inhibition of blebbing is possible because the compressive stress applied by local contraction of the actino-myosin cortex is dissipated over a length-scale of a few microns. When the cells are locally treated with actin depolymerising drugs, bleb sizes increase globally. Actin depolymerisation leads both to an increase in pore size and a decrease in bulk elasticity [8,9], which are competing effects in the expression of D. An increase in D would mean that stresses diffuse faster and have an effect further away from their initiation. This would lead to a global increase in bleb size even though the treatment is local. It is important to note that our poroelastic description points towards a new treatment of all cytoplasmic mechanical behavior that involves rapid relative motions of its constituent fluid and solid components.

Starting with this picture for stress generation, the critical area of membrane detachment from the cytoskeleton needed for a bleb to start growing can be estimated. The free energy for the detachment of a small area of membrane of diameter d from the cortex, is $U \approx Pd^2\delta - Jd^2 - T\delta^2$ where P is the given hydrostatic pressure, δ the membrane deflection, J the membrane-cytoskeleton adhesion energy, and T the membrane tension. For small deflections, the membrane unwrinkles as it detaches, and can flow in the plane to accommodate blebbing. Therefore, the membrane tension is relatively uniform as the bleb starts forming, hence $T \approx T_0 \approx$ constant . In this limit, solving $\frac{\partial U}{\partial d} = \frac{\partial U}{\partial \delta} = 0$ yields the critical bleb size $d_c \sim (\frac{T_0 J}{P^2})^{1/2}$ above which a bleb will grow catastrophically in a pressure controlled situation; however, the limited volume of fluid available prevents this. Equating this critical size to the average distance between cytoskeletal-membrane anchors yields the minimum pressure for bleb growth. With J~10^{-4} J.m^{-2} [10], T_0~10^{-2} mN.m^{-1} [11], and P~300 Pa (Figure S1), we get a nucleation size d_c~100nm.

Finally, during retraction, myosin heads moving along actin filaments bring the bleb back towards the cell body forcing the cytosol back in. Assuming a constant pressure within the bleb because it only consists of cytosol, Darcy's law implies that the cortex must exert a pressure $\Delta P \approx \frac{vd}{k}$ with v the retraction speed , d the stress diffusion length, and k the hydraulic permeability of the cytoskeleton. Applying the Laplace law, the cortical tension T_c due to actino-myosin contraction is $T_c \sim \Delta P.R_b \sim \frac{vdR_b}{k}$. Assuming a homogeneous distribution of myosin motors in the hemispherical cortical shell, this implies that the force generated by the motors scales as $F \sim T_c R_b$.

Therefore, the number of working motors is roughly $N \sim \frac{vdR_b^2}{kf_{myo}\omega_{myo}}$ where f_{myo}~1.5 pN [12,13] is the force per myosin motor per cycle, ω_{myo}~25 Hz [14] is the myosin motor cycle frequency. With d~8 µm, v~0.1 µm.s^{-1} (Figure 1D and S2) , k~3.4 10^{-15} m^4.N^{-1}.s^{-1} and R_b~5 µm, we get N~350 myosin heads. This is a realistic number in view of the estimated number of myosins within a cell N_{total}>10^4 [15].

Supplementary results

Blebbing is an isochoric phenomenon

Maintenance of cell volume during blebbing was assessed by measuring the volume of blebbing cell fragments over time.

Cell fragments (microplasts) are capable of autonomous behaviours, and in particular blebbing [16] (Supplementary video 12). Whereas blebs represent at most 0.5% of the cell volume in a blebbing cell, in microplasts they represent up to 15% of the fragment volume. Therefore, we chose to assess volume fluctuations over time in microplasts rather than in whole cells. The amplitude of volume fluctuations of blebbing microplasts were on average 6.8±2.6% (N=12 microplasts, 16 measurements, Supplementary figure S4), not significantly different from the resolution of our measurement method ($p=0.54$). In contrast, the relative volume increase expected, if blebbing were due to an increase in volume, was on average 17.5±11.2%, which was significantly larger than the estimated measurement errors (7.65±4.0%, $p<0.001$). Hence, blebbing is not accompanied by an increase in cell volume, in agreement with previous work[3].

Supplementary Methods

Cell Culture

Cells were cultured in MEM with Earle's salts (Invitrogen, Carlsbad, CA) with Penicillin Streptomycin, 0.01 M HEPES, and 10% 80:20 mix of donor calf serum:foetal calf serum. For local perfusion assays, the cells were trypsined, plated on 40x22 mm #1 glass coverslips and cultured overnight in an incubator.

High-Throughput Screen

High-throughput screening for known bioactive inhibitors of blebbing was performed as described in [17]. Briefly, cells were plated in 384 well plates at a volume of 40 µl per well and a concentration of 2.10^5 cells.ml^{-1} and cultured in an incubator for 2h prior to screening. The effects of a library of 489 known bioactive compounds was examined (List available at iccb.med.harvard.edu/screening/compound_libraries/bioactives_collection1.htm). Chemical compounds (20 or 40 nl) were transferred into wells of the plate using a steel pin array. The plates were then transferred to the incubator and the inhibitors were left to act for 10 min. The cells were then fixed by addition of a solution of MEM containing 2% formaldehyde and 0.1% glutaraldehyde for 15 min. The cells were washed twice in TBS and stained for 15 min with NHS-ester (a general protein marker) in TBS with 0.1% Triton X. The cells were then washed twice and stained with the nucleic acid stain Hoechst-33342 (Sigma, St-Louis, MO) for 1 min. The cells were washed in TBS one final time.

Automated imaging was performed on a NikonTE300 (Nikon corp., Tokyo, Japan) inverted fluorescence microscope with filter wheel (Sutter Lamda10-2, Sutter instrument company, Novato, CA), x-y stage (Prior H107N300, Prior scientific, Rockland, MA), and piezoelectric-motorized objective holder (Physik Instrumente P-723.10, Physik intrumente, Karlsruhe, Germany). Images were captured on a CCD camera (Hamamatsu OrcaER, Hamamatsu, Hamamatsu city, Japan) and transferred to

a PC running Metamorph software (Universal Imaging Corporation, Downingtown, PA) that allows coordination of software-based auto-focusing, movement between wells, imaging, and image evaluation. Images were acquired using a 10x objective with 2x2 binning. All experiments were performed in duplicate for two different concentrations (20 or 40 nl of compound transferred). The images were examined in double-blind and graded for efficacy. Compounds that inhibited blebbing were reordered from the suppliers.

Bulk inhibitor treatment

After the screen had been effected, the minimal concentration needed for each compound to inhibit blebbing was determined by dilution series and time-lapse DIC microscopy. During a typical experiment, ~30 images (~150s) were acquired prior to drug exposure to ensure that the cells did bleb. The cells were then exposed to drug for ~70 images (~350s), and allowed to recover for 20 frames (~100s). Time-lapse microscopy of the experiments was performed on a NikonTE300 inverted fluorescence microscope with filter wheel. Images were acquired every 5s with a 20x objective on a CCD camera with a 2x2 binning and transferred to a PC computer running Metamorph software. Exposure times were ~200 ms for DIC images. All experiments were performed at 37ºC in Leibovitz-L15 medium with 10% 80:20 mix of donor calf serum:foetal calf serum.

Osmolarity series and data processing

For treatment with sucrose to increase osmolarity, cells (N=8) were exposed to increasing concentrations of sucrose in the following order: Control, 1, 5, 10, 50, 100, 150, and 300 mM. For the hypotonic series, the cells (N=7) were exposed to increasingly dilute solutions in the following order: 5, 10, 20, 30, 40, and 50 % dH_20. The cells were exposed to each condition for 150s and images were taken every 5s. Bleb diameters were measured using Metamorph. For each sucrose concentration, bleb sizes were measured after the cells were given 50s to adapt to the change in osmolarity. Bleb diameters and frequency were normalised to the control diameters and frequency for each cell. The increase in osmotic pressure relative to the original solution was calculated as P_{osm}=[Sucrose].R.T with R the universal gas constant R=8.314 $J.mol^{-1}.K^{-1}$, and T=300K. For hypotonic series, the decrease in osmotic pressure was calculated as $P_{osm}=P_0(1-\%H_2O)$.

Plasmids and transfection

Actin localization was visualized by transfecting the cells with an adenovirus containing GFP-tagged human beta actin. For myosin localization, the cells were transfected with GFP or RFP-tagged Xenopus myosin II regulatory light chain (MRLC) (a kind gift from Dr. Aaron Straight). The membrane was visualized by transfecting the cells with the PH domain of phospholipase-Cδ tagged with GFP or RFP (a kind gift from Dr. Tamas Balla). GFP-C1 (Clontech) was used as a cytoplasmic marker in volume fluctuation experiments. Plasmid transfections were effected using lipofectamine Plus (Invitrogen).

Microscopic examination of transfected cells and image processing

Transfected cells were examined on a Nikon TE2000 inverted microscope equipped with a Prior scientific motorised stage interfaced to an Ultraview Perkin-Elmer spinning disk confocal microscope. Images were captured on a Hamamatsu Orca ER CCD camera and acquired on a PC using Metamorph software. Images of the cells were acquired at 2s intervals for several minutes.

Microplast preparation, volume fluctuation assessment, and relative bleb volume estimation

Microplasts were prepared as described previously [16], except that they were transfected with GFP to act as a cytoplasmic marker. On the day of the experiment, the cells were then incubated with 5 $\mu g.ml^{-1}$ cytochalasin D for 1h at 37ºC. The cells were then broken into fragments by harsh pipetting, washed twice with medium, and left to reheal for 30 min. They were then trypsined and replated onto coverglasses for 1h prior to examination. This yielded cell fragments ranging in size from 4-10 μm that blebbed extensively (Figure S4B).

The volume of the GFP transfected microplasts was estimated by taking multiple confocal slices ($N \geq 5$) through the microplast at intervals of 0.5 to 1 μm, the area of each optical slice was estimated, and the sum of the areas was multiplied by the thickness of an optical section to obtain an estimated of the volume. To measure the area of a given slice, a histogram plot of the intensities was generated, and a gaussian was fit to the histogram. The main peak in any image represented the background pixels. Pixels whose intensity was superior to the value of the peak of the gaussian plus eight standard deviations were considered signal. The volume evolution was computed and normalised to the average volume of the first five time points. Photobleaching of GFP was apparent from the time-lapse movies due to the the small volume of the microplasts and was accounted for by fitting a straight line to the volume evolution. The volume fluctuations were taken to be the difference between the experimental volume curve and the line-fit.

For each microplast, the volume of a representative bleb was estimated by measuring its radius and assuming it was a sphere. The bleb volume relative to the measured microplast volume was computed. The number of simultaneously growing blebs was determined from visual inspection of the videos. Finally, the relative volume of growing blebs was compared the largest amplitude of volume fluctuation measured.

Measurement errors were estimated as follows. For the top slice or the bottom slice, the average error was taken to be $\varepsilon \cong \frac{Adz}{4} + 2\pi \frac{dx}{2}\frac{dz}{2}\sqrt{\frac{A}{\pi}}$ with A the area, dz the depth of the confocal slice, dx the resolution in x and y. There are two contributions to the average error. The first is the underestimation of the volume because of a dz/2 incertitude in the location of the cell boundary. This error is counted only once for the top and bottom slice yielding, on average, a ¼ factor. The second contribution is the error commited on the location of the cell boundary due to the limited resolution in x and y (0.13 μm), and the optical section thickness in z. To estimate this, we assumed that the cell was circular with an area A in any given optical section. For intermediate

slices, only the second term contributes to the average error. Measurement errors decreased with increasing numbers of optical slices and with increasing volume. Only microplasts with expected volume increases larger than the estimated measurement error were analysed because they are the only ones for which we could hope to reliably observe a volume increase.

The expected volume changes were compared to the measured volume fluctuation amplitude and error estimates. The measured volume fluctuation amplitude was compared to the error estimate. Two tailed t-tests were used for all statistical comparisons and the significance level was taken to be 0.01.

Network Elasticity Measurement

Elasticity measurement were performed by Atomic force microscope (AFM) micro-indentation and analysed as described in [18]. All of the measurements were effected on cells incubated in L15 medium with 10% 80:20 mix of donor calf serum: foetal calf serum and 300 mM sucrose. The hypertonic conditions for the measurements were selected to reduce the impact of cytosol on the apparent elasticity. Briefly, four force-distance curves were collected at the four apices of a 1x1 μm square on the top of the cell using a Thermomicroscopes Explorer AFM (Veeco instruments, Woodbury, NY). The measurements were carried out using a soft V-shaped cantilever with a pyramidal tip (k=0.067 $N.m^{-1}$, calibrated in air prior to experimentation, model MCL-XT-A, Veeco). For each curve, the cellular material properties were evaluated as described in [19]. The cell was assumed to be a homogenous half space and the AFM tip conical. The force F needed to produce an indention of depth δ in a half-plane with an elastic modulus E is [20]:

$$F_{conical} = \frac{2}{\pi} \frac{E}{(1-\nu^2)\tan(\alpha)} \delta^2$$

With α the opening angle of the conical tip and ν the local Poisson ratio. Knowing the cantilever stiffness and by fitting the theoretical curve to the experimental data, the elastic modulus can be deduced [19]. The cellular Poisson ratio was assumed to be 0.5, and the conical tip opening was taken to be 30º.

The average elastic modulus derived from these experiments was K=2137±1277 Pa.

Supplementary Table 1

Drugs used in local perfusion experiments. The drug target was determined from the existing literature and vendor catalogs. The bulk concentration is the concentration needed to inhibit blebbing when the whole cell was bathed in medium with inhibitor. The concentration in the pipette refers to the concentration needed in the micropipette to observe inhibition of blebbing when the whole cell is treated by local drug perfusion. Local effect refers to whether a drug can locally inhibit blebbing or not. Global effect describes the effect observed when the cell is treated in bulk.
Abbreviations: PKA, PKC, PKG: protein kinase A, C, G; MLCK: myosin light chain kinase; CamK: calmodulin kinase

Treatment	Target	Concentration in bulk	Concentration in pipette	Global effect	Local effect	References (Global effect)	Supplier
Blebbistatin	Myosin II ATP-ase	50 μM	100 μM	Arrests bleb protrusion	Yes	[21]	Tocris
3-(4-pyridyl)indole	Rho-kinase	50 μM	200 μM	Arrests bleb protrusion	Yes	[22]	ICCB
Y-27632	Rho-kinase	1 μM	12.5 μM	Arrests bleb protrusion	Yes	[23]	Calbiochem
Sucrose	Osmotic pressure	300 mM	300 mM	Decreases bleb size	Yes	[24]	JT Baker
WGA	Membrane bending rigidity	0.1 $mg.ml^{-1}$	0.1 $mg.ml^{-1}$	Arrests bleb protrusion	Yes	[25]	Molecular Probes
Dilute solution	Osmotic pressure	50% dH_2O	50% dH_2O	Increases bleb size	Yes	[24]	
Latrunculin B	F-actin	7.5 μM	7.5 μM	Increases bleb size, arrests bleb protrusion, arrests retraction	Yes		Calbiochem
Cytochalasin D	F-actin	5 μM	10 μM	Increases bleb size, arrests bleb protrusion, arrests retraction	Yes	[26]	Calbiochem
Staurosporine	PKA, PKC, PKG, CamK, MLCK	1 μM	5 μM	Arrests bleb protrusion	No		Calbiochem
HA-1077	Ca^{2+} antagonist, PKA, PKG, PKC, MLCK, ROCK	5 μM	10 μM	Arrests bleb protrusion	No		Tocris
H-9	PKA, PKC, PKG	10 μM	50 μM	Arrests bleb protrusion	No		Tocris
H-89	PKA, PKC, CamK, MLCK		20 μM	Arrests bleb protrusion	No		Calbiochem

Supplementary Video 1 - Bath treatment of cells with high concentration sucrose

This video shows the treatment of a cell with increasing concentrations of sucrose. As the concentration increases, bleb size decreases until finally blebbing ceases and the cell switches to ruffling.

Supplementary Video 2 - Bath treatment of cells with WGA

This video shows the treatment of a cell with increasing concentrations of WGA. As the concentration of WGA in the medium increases, blebs become rarer until blebbing finally stops.

Supplementary Video 3 –Local perfusion of WGA

This video shows the time course of the experiment depicted in Figure 2A. Prior to application of treatment, the cells blebbed profusely around their periphery. Within 2-3 min of application, blebbing ceases in the area of application but continues undisturbed in the rest of the cell. Solid black lines delineate the flow out of the micropipette.

Supplementary Video 4 – Local perfusion of Sucrose

This video shows the time course of the experiment depicted in Figure 2B. Prior to application of treatment, the cells blebbed profusely around their periphery. Within 2-3 min of application, blebbing ceases in the area of application but continues undisturbed in the rest of the cell. Solid black lines delineate the flow out of the micropipette.

Supplementary Video 5 – Local perfusion of Blebbistatin

This video shows the time course of the experiment depicted in Figure 2C. Prior to application of treatment, the cells blebbed profusely around their periphery. Within 2-3 min of application, blebbing ceases in the area of application but continues undisturbed in the rest of the cell. Solid black lines delineate the flow out of the micropipette.

Supplementary Video 6 – Local perfusion of 3-(4-pyridyl)indole

This video shows the time course of the experiment depicted in Figure 2D. Prior to application of treatment, the cells blebbed profusely around their periphery. Within 2-3 min of application, blebbing ceases in the area of application but continues undisturbed in the rest of the cell. Solid black lines delineate the flow out of the micropipette.

Supplementary Video 7 – Local perfusion of Latrunculin

This video shows the time course of the experiment depicted in Figure 3A. Prior to application of treatment, the cells blebbed profusely around their periphery. When Latrunculin B is applied locally, bleb size increases globally. Within 2-3 min of application, blebbing ceases in the area of application but continues undisturbed in the rest of the cell. Solid black lines delineate the flow out of the micropipette.

Supplementary Video 8 – Local perfusion of Staurosporine

This video shows the time course of the experiment depicted in Figure 3B. Prior to application of treatment, the cells blebbed profusely around their periphery. Prior to perfusion and after 395 s of local perfusion with Staurosporine, blebbing is unperturbed throughout the cell. When Staurosporine is applied to the whole cell, blebbing ceases. Solid black lines delineate the flow out of the micropipette.

Supplementary Video 9 – Local perfusion of HA 1077

This video shows the time course of the experiment depicted in Figure 3C. Prior to application of treatment, the cells blebbed profusely around their periphery. After 340s of local HA-1077 application, blebbing is unperturbed. When the whole cell is exposed to inhibitor, blebbing ceases. When perfusion is halted, blebbing is restored. Solid black lines delineate the flow out of the micropipette.

Supplementary Video 10 – Colocalisation of actin and myosin II at the cell cortex

This video shows a time course of a blebbing cell transfected with actin-GFP and MRLC-RFP. The colours have been inverted on the video to render viewing easier. Actin is in red, and MRLC in green. Colocalisation appears in yellow and can clearly be observed at the cortex. Frames are 5s apart.

Supplementary video 11 – MRLC localisation during blebbistatin treatment

This video shows the localisation of MRLC during blebbistatin treatment. After 150s, 100 μM blebbistatin is applied to the cell. Blebbistatin treament causes MRLC to detach from the cortex and relocalise to the cell membrane.

Supplementary video 12 – Blebbing microplast

This video shows the time course of a blebbing GFP transfected microplast from Supplementary Figure S4. Frames are 5s apart.

Supplementary Figure 1 – Dose response of bleb diameter and frequency with increasing osmotic pressure

Normalized bleb diameter and bleb frequency decrease with increasing osmotic pressure. The normalized bleb diameter shows a rapid decrease with increasing osmotic pressure from ~100 Pa; whereas bleb frequency stays unaffected until pressures of ~300 Pa. When cells are exposed to hypoosmotic medium, bleb size increases and bleb frequency decreases. The error bars denote the standard deviation of each measurement. The dotted line indicates the control osmolarity.

Supplementary Figure 2 – Distribution of maximum bleb expansion velocities and minimum bleb retraction velocities.

A. Retraction velocities followed a normal distribution with a maximum peak for $0.1\ \mu m.s^{-1}$.
B. Expansion velocities followed a normal distribution with a maximum peak for $0.4\ \mu m.s^{-1}$.

Supplementary Figure 3 – Dissassembly of the actin cortex posterior to bleb expansion

Time course of the plasma membrane and actin cortex during bleb expansion. The plasma membrane (in red) and actin (in green) were visualized by transfecting the cells with actin-GFP and PH-PLCδ-RFP. Scale bar=2µm.
Originally, the plasma membrane lies in close proximity to the actin cortex (t=0s). As bleb expansion proceeds, the membrane detaches from the cortex, which appears to remain intact (t=6s and t=12s). Once expansion is halted, the cortex is disassembled and a new cortex is reformed underneath the bleb membrane (t=24s).

Supplementary Figure 4 – Volume Fluctuations in a blebbing microplast

A- Volume fluctuations (in %) over time for the microplast shown in Supplementary Video 12. The maximal amplitude of fluctuations was 4.5%. The estimated error on the volume measurement was 5.9%. Up to 2 expanding blebs appear simultaneously, with a representative diameter of 4 µm. The volume represented by those two blebs was 17% of the microplast volume. This is clearly larger than the observed fluctuations.

B- Projection image of the GFP transfected microplast from A and supplementary video 12.

Supplementary Figure 1

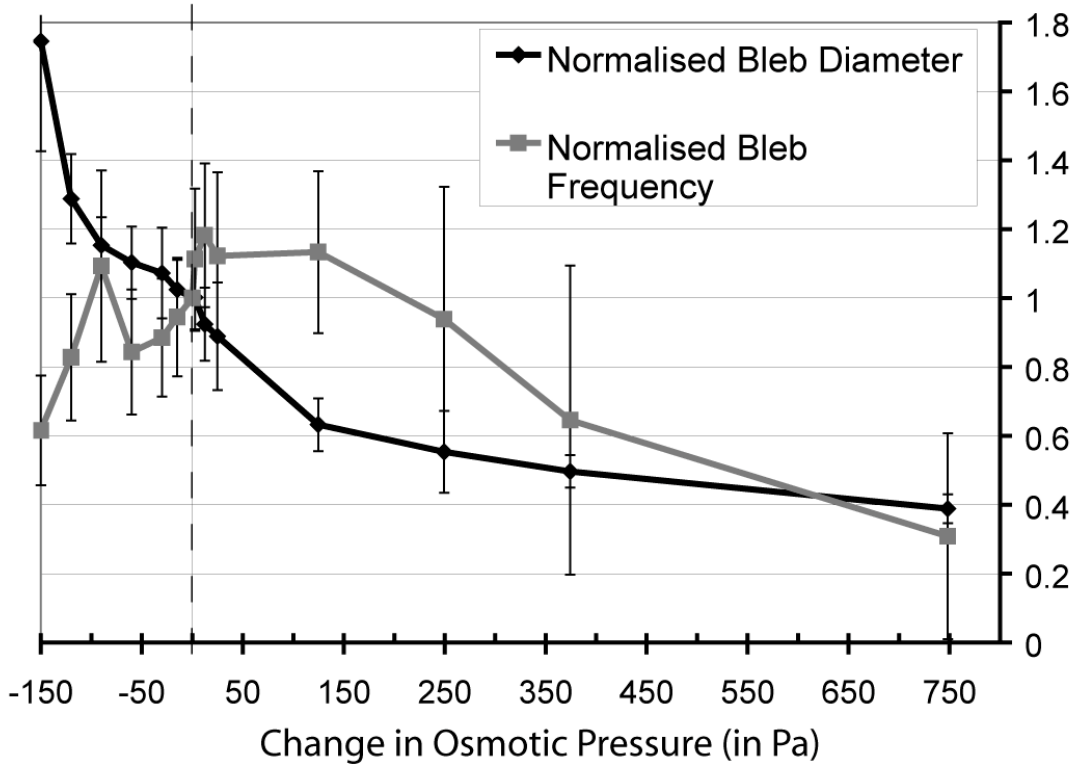

Supplementary Figure 2

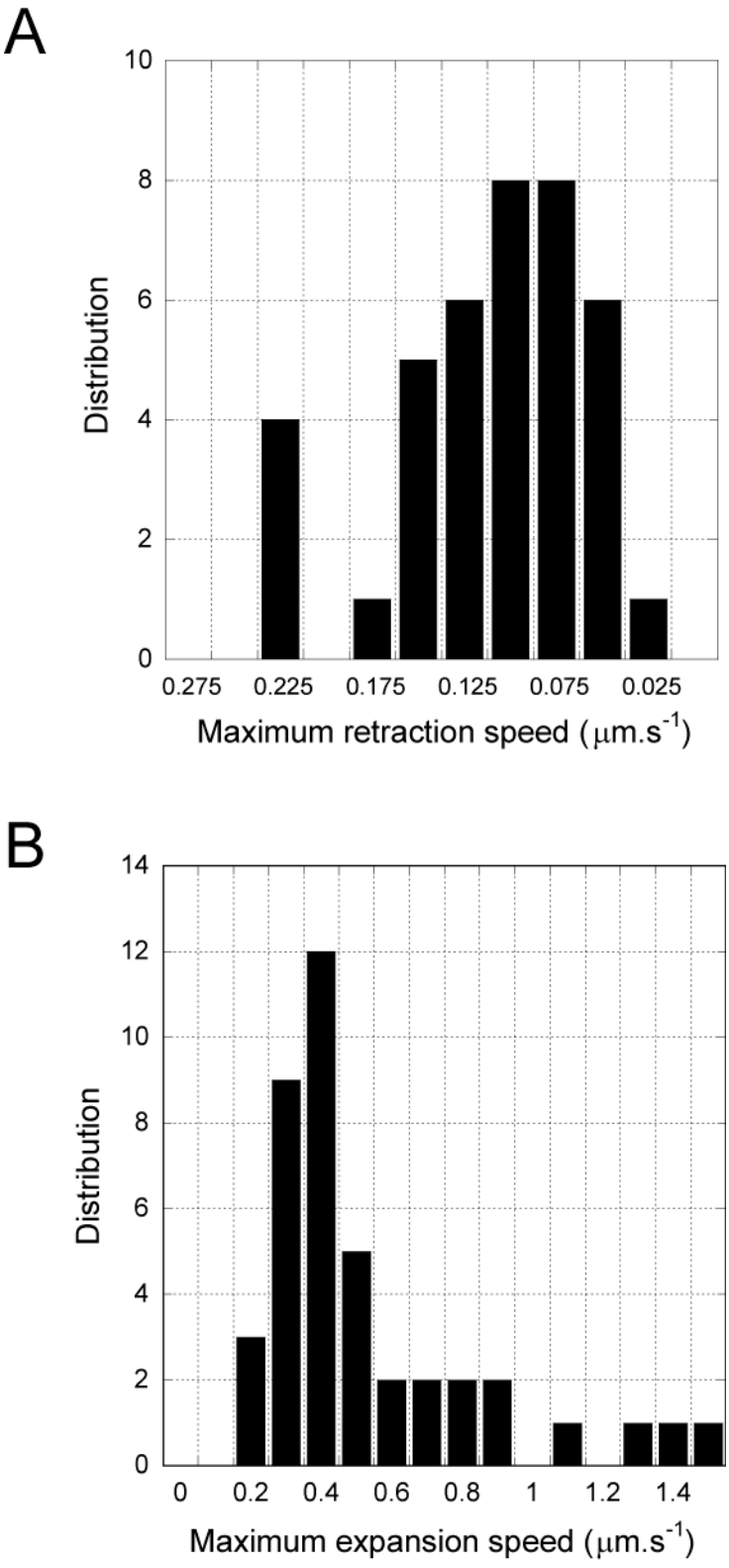

Supplementary Figure 3

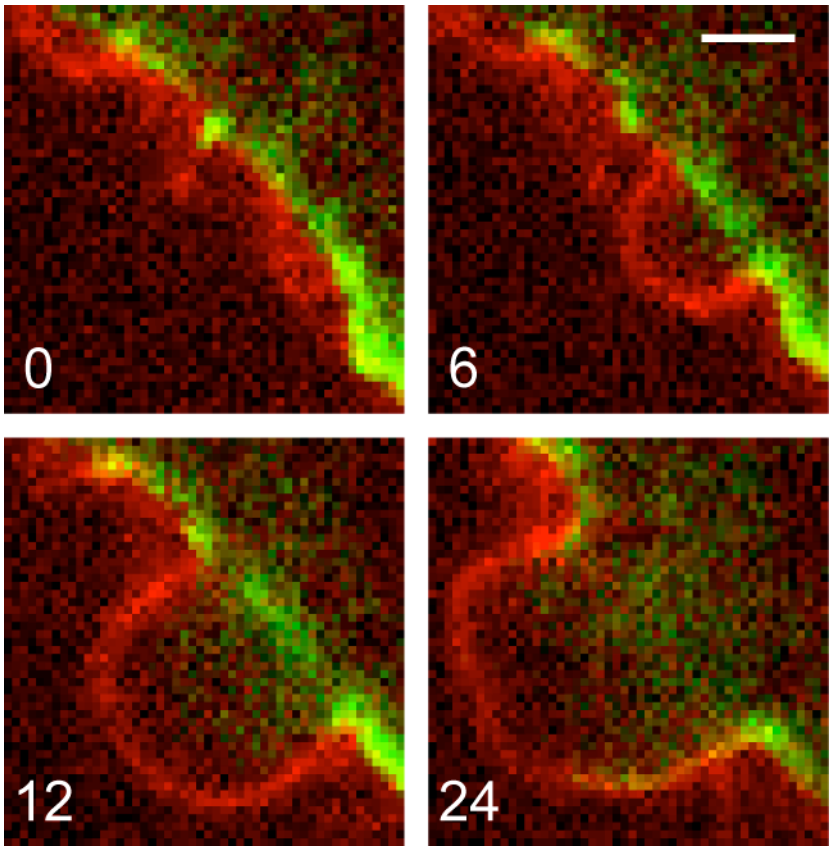

Supplementary Figure 4

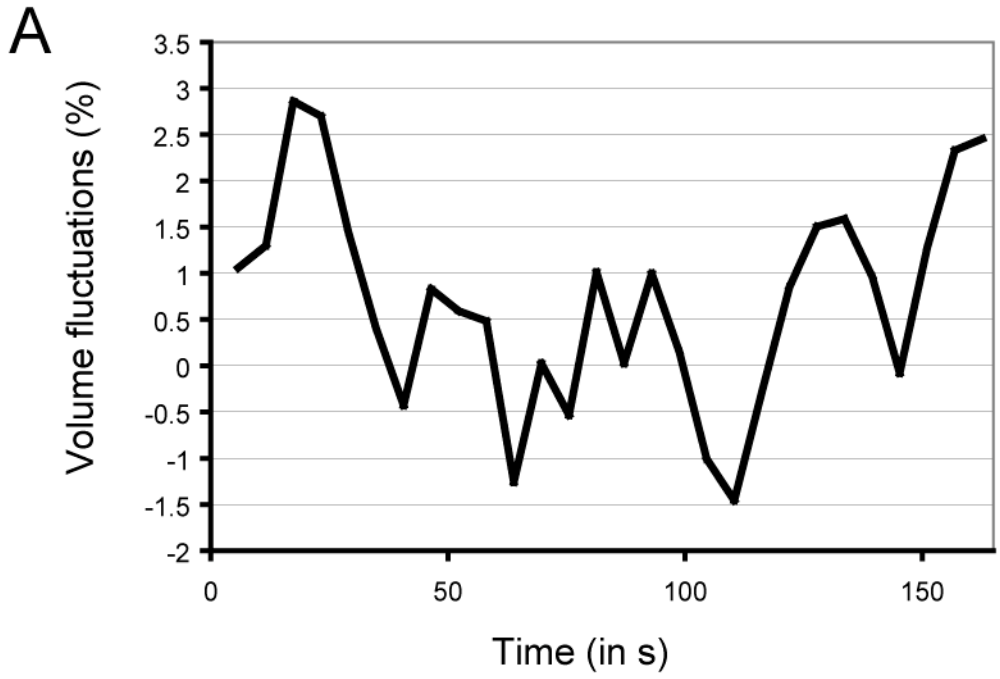

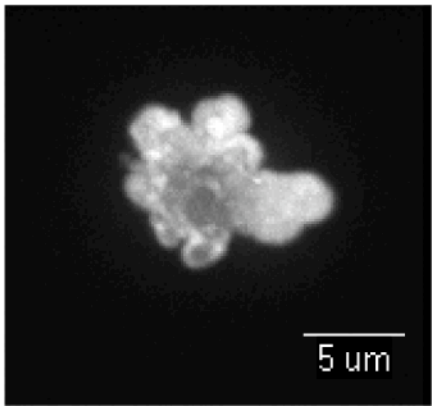

References

1. Skotheim, J. and Mahadevan, L., Dynamics of poroelastic filaments. *Proc. R. Soc. Lond (A),* **460,** 1995-2020 (2004).
1. Mastro, A. M. & Keith, A. D. Diffusion in the aqueous compartment. *J Cell Biol* **99**, 180s-187s (1984).
2. Kao, H. P., Abney, J. R. & Verkman, A. S. Determinants of the translational mobility of a small solute in cell cytoplasm. *J Cell Biol* **120**, 175-84 (1993).
3. Albrecht-Buehler, G. Does blebbing reveal the convulsive flow of liquid and solutes through the cytoplasmic meshwork? *Cold Spring Harb Symp Quant Biol* **46 Pt 1**, 45-9 (1982).
4. Flanagan, L. A. et al. Filamin A, the Arp2/3 complex, and the morphology and function of cortical actin filaments in human melanoma cells. *J Cell Biol* **155**, 511-7 (2001).

5. Luby-Phelps, K., Castle, P. E., Taylor, D. L. & Lanni, F. Hindered diffusion of inert tracer particles in the cytoplasm of mouse 3T3 cells. *Proc Natl Acad Sci U S A* **84**, 4910-3 (1987).
6. Weiss, M., Elsner, M., Kartberg, F. & Nilsson, T. Anomalous subdiffusion is a measure for cytoplasmic crowding in living cells. *Biophys J* **87**, 3518-24 (2004).
7. Alexopoulos, L. G., Erickson, G. R. & Guilak, F. A method for quantifying cell size from differential interference contrast images: validation and application to osmotically stressed chondrocytes. *J Microsc* **205**, 125-35 (2002).
8. Rotsch, C. & Radmacher, M. Drug-induced changes of cytoskeletal structure and mechanics in fibroblasts: an atomic force microscopy study. *Biophys J* **78**, 520-35 (2000).
9. Charras, G. T. & Horton, M. A. Single cell mechanotransduction and its modulation analyzed by atomic force microscope indentation. *Biophys J* **82**, 2970-81 (2002).
10. Moy, V. T., Jiao, Y., Hillmann, T., Lehmann, H. & Sano, T. Adhesion energy of receptor-mediated interaction measured by elastic deformation. *Biophys J* **76**, 1632-8 (1999).
11. Dai, J., Sheetz, M. P., Wan, X. & Morris, C. E. Membrane tension in swelling and shrinking molluscan neurons. *J Neurosci* **18**, 6681-92 (1998).
12. Molloy, J. E., Burns, J. E., Kendrick-Jones, J., Tregear, R. T. & White, D. C. Movement and force produced by a single myosin head. *Nature* **378**, 209-12 (1995).
13. Tyska, M. J. et al. Two heads of myosin are better than one for generating force and motion. *Proc Natl Acad Sci U S A* **96**, 4402-7 (1999).
14. Howard, J. *Mechanics of Motor Proteins and the cytoskeleton* (Sinauer associates, 2001).
15. Evans, E., Leung, A. & Zhelev, D. Synchrony of cell spreading and contraction force as phagocytes engulf large pathogens. *J Cell Biol* **122**, 1295-300 (1993).
16. Albrecht-Buehler, G. Autonomous movements of cytoplasmic fragments. *Proc Natl Acad Sci U S A* **77**, 6639-43 (1980).
17. Yarrow, J. C., Feng, Y., Perlman, Z. E., Kirchhausen, T. & Mitchison, T. J. Phenotypic screening of small molecule libraries by high throughput cell imaging. *Comb Chem High Throughput Screen* **6**, 279-86 (2003).
18. Charras, G. T. & Horton, M. A. Determination of cellular strains by combined atomic force microscopy and finite element modeling. *Biophys J* **83**, 858-79 (2002).
19. Radmacher, M. Measuring the elastic properties of biological samples with the AFM. *IEEE Eng Med Biol Mag* **16**, 47-57 (1997).
20. Johnson, K. L. *Contact Mechanics* (Cambridge University Press, 1985).
21. Cheung, A. et al. A small-molecule inhibitor of skeletal muscle myosin II. *Nat Cell Biol* **4**, 83-8 (2002).
22. Yarrow, J. C., Totsukawa, G., Charras, G. T. & Mitchison, T. J. Screening for cell migration inhibitors using automated microscopy reveals a new rho-kinase inhibitor. *Manuscript in preparation* (2004).
23. Mills, J. C., Stone, N. L., Erhardt, J. & Pittman, R. N. Apoptotic membrane blebbing is regulated by myosin light chain phosphorylation. *J Cell Biol* **140**, 627-36 (1998).

24. Dai, J. & Sheetz, M. P. Membrane tether formation from blebbing cells. *Biophys J* **77**, 3363-70 (1999).
25. Evans, E. & Leung, A. Adhesivity and rigidity of erythrocyte membrane in relation to wheat germ agglutinin binding. *J Cell Biol* **98**, 1201-8 (1984).
26. Cunningham, C. C. Actin polymerization and intracellular solvent flow in cell surface blebbing. *J Cell Biol* **129**, 1589-99 (1995).